Steel and Composite Structures, *Vol. 20, No. 2 (2016) 295-316*
DOI: http://dx.doi.org/10.12989/scs.2016.20.2.295

Axial compression ratio limit values for steel reinforced concrete (SRC) special shaped columns

Zongping Chen [*1,2], Jinjun Xu [**1a], Yuliang Chen [1] and Jianyang Xue [1]

[1] *College of Civil Engineering and Architecture, Guangxi University, Nanning, 530004, P.R. China*
[2] *Key Laboratory of Disaster Prevention and Structural Safety of Chinese Education Ministry, Guangxi University, Nanning, 530004, P.R. China*

(*Received January 23, 2015, Revised May 12, 2015, Accepted October 28, 2015*)

Abstract. This paper presents the results of experimental investigation, numerical calculation and theoretical analysis on axial compression ratio limit values for steel reinforced concrete (SRC) special shaped columns. 17 specimens were firstly intensively carried out to investigate the hysteretic behavior of SRC special shaped columns subjected to a constant axial load and cyclic reversed loads. Two theories were used to calculate the limits of axial compression ratio for all the specimens, including the balanced failure theory and superposition theory. It was found that the results of balanced failure theory by numerical integration method cannot conform the reality of test results, while the calculation results by employing the superposition theory can agree well with the test results. On the basis of superposition theory, the design limit values of axial compression ratio under different seismic grades were proposed for SRC special shaped columns.

Keywords: steel reinforced concrete (SRC); special shaped column; axial compression ratio; limit; hysteretic behavior; balanced failure theory; superposition theory; numerical integration

1. Introduction

Special shaped column is a column with L-shaped, T-shaped, cross (+)-shaped or Z-shaped cross-sections, which is located in the corner of frame structures, and its advantage is saving the indoor space and convenient for the furniture arrangement (Wu and Xu 2009, Xu and Wu 2009, Zhou *et al*. 2012, Patton and Singh 2012). In past decades, reinforced concrete (RC) special shaped columns have been extensively studied. Ramamurthyhe and Khan (1983), Marin (1979), Wsu (1985) and Hsu (1989) provided the computer calculation methods for RC L-shaped columns, including the methods of ultimate bearing capacity, load-bending moment curve and the relationship between bending moment and curvature. From 1990's to the beginning of 2000's, many scholars such as Mallikarjuna and Mahadevappa (1992), Tsao and Hsu (1993), Dundar and Sahin (1993), Yau *et al*. (1993), Sinha (1996) started to make computer programs for different kinds of special shaped columns to calculate their bearing capacities under biaxial eccentric compression. Several researchers, including Kang and Gong (1997), Li *et al*. (2002), Zhao *et al*.

*Corresponding author, Ph.D., E-mail: zpchen@gxu.edu.cn
**[a] Ph.D. Student, E-mail: jjxu_concrete@163.com

Copyright © 2016 Techno-Press, Ltd.
http://www.techno-press.org/?journal=scs&subpage=6 ISSN: 1229-9367 (Print), 1598-6233 (Online)

(2004) and Cao *et al*. (2005) carried out experimental investigations to reveal the seismic behavior of RC special shaped columns, and the test results indicated that the main seismic indexes (shear bearing capacity, energy-dissipation, ductility, etc.) of these columns were inferior to those of rectangle RC columns.

Up to now, with the development of architectural structural system, steel-concrete (SC) composite structures start to show their stronger performance and better economic advantages compared with RC structures. Due to the limitation of RC materials, the special shaped columns composed of shape steel and RC named steel reinforced concrete (SRC) special shaped columns and the special shaped columns composed of concrete filled steel tube named CFST special shaped columns were proposed by Xue *et al*. (2012) and Zuo *et al*. (2012b), respectively. Later, Wang and Chang (2013) carried out a numerical study of axially loaded T-shaped CFST columns based on ABAQUS software, and then proposed a simplified formulae for designing. Considerable works were carried out to describe the behavior of eccentrically loaded the steel fibre high strength RC columns. Therefore, based on the before-mentioned consideration, Tokgoz and Dundar (2012) developed a new kind of steel-RC composite special shaped column – L-shaped steel fibre high strength RC composite column, and then to test their biaxial bending performance as well as the behavior under the short-term axial compression.

It is vital to ensure certain requirements of ductility for a structure subjected to the seismic-induced action when it is in the point of failure state. As a matter of fact, axial compression ratio n is one of the key factors for controlling the structural ductility. Two Chinese criterions, including Code for seismic design of buildings (GB 50011-2010 2010) and Technical specification for concrete structures with specially shaped columns (JGJ149-2006 2006), list the calculation method of axial compression ratio for RC special shaped columns

$$n = N/(f_c A) \tag{1}$$

where N is the vertical load, f_c is the compressive strength of concrete prism ($f_c = 0.76 f_{cu}$), f_{cu} is the cubic compressive strength of the column concrete (the side length of the standard cubic specimens = 150 mm), A is the full sectional area of a column.

In addition, the design method of axial compression ratio for SRC structural columns is provided according to Technical specification for steel reinforced concrete composite structures (JGJ 138-2001 2001) and Technical specification of steel-reinforced concrete structures (YB 9082-2006 2007)

$$n = N/(f_c A_c + f_s A_{ss}) \tag{2}$$

where A_c is the sectional area of column concrete, A_{ss} is the sectional area of shape steels, f_s is the tensile yield strength of shape steel.

In spite of the excessive studies in the literature, the topics on the limit value of axial compression ratio and its design method for SRC special shaped columns still have not been fully addressed, since all the calculation methods and specification requirements in the previous researches are only focusing on the rectangular RC/SRC columns and RC special shaped columns.

In this paper, low cyclic reversed loading tests on 17 specimens were firstly conducted to investigate the hysteretic performance of SRC special shaped columns. The load-displacement hysteretic relationships and deformation characteristics of the test subassemblies were discussed in detail; in addition, the development of concrete cracking and failure modes of the specimens are concentrated on. Furthermore, two theories were used to derive the limit values of axial

compression ratio for the specimens, including the balanced failure theory and superposition theory. Finally, the proposed methods in this paper are verified by the experimental results.

2. Experimental program

2.1 Specimen preparations and material properties

A total of 17 specimens of SRC special shaped columns, including nine T-shaped columns, four L-shaped columns and four cross-shaped columns were constructed in the research program. The experimental parameters illustrated below were the shape steel configuration, loading angle, axial compression ratio and shear-span ratio.

(1) Steel form in column cross-section: three kinds of shape steels configured were the T-shaped steel, channel-shaped steel and solid-web steel. Both T-shaped steel and channel-shaped steel in this study can be named empty-web steel to differentiate from the solid-web steel. The diameter of 6 mm of longitudinal steel reinforcement bar was used in all specimens, and the reinforcement stirrup was the iron wire with Chinese Standard No.8 (4.0 mm in diameter). The steel flat (or steel web member) with cross-section of 25 mm (height) × 8 mm (width) was used to connect the steel plates in the specimens configured with T-shaped steel and channel steel.

(2) Loading angle: for the T-shaped columns, three kinds of loading angles were selected to study the seismic-induced failure mechanism of test specimens, including loading along the web, flange and 45° angle; while for the L-shaped and cross-shaped columns, it was the engineering axis and 45° angle that were adopted for loading. Fig. 1 shows the planar and spatial loading diagrams of loading angles for specimens.

(3) Test axial compression ratio $n^t = N^t / (f_c^t A)$ was used to reveal the effect of axial compression ratio on the seismic behavior of SRC special shaped columns, where N^t is the vertical load simulating the axial pressure in the test, f_c^t is the test compressive strength of concrete prism ($f_c^t = 0.76 f_{cu}$), the mechanical properties of concrete listed in Table 1 are obtained on the same day of testing specimens, A is the full sectional area of the column.

(4) Shear-span ratio ($\lambda = L/(2h)$): in order to simulate various working conditions, the shear-span ratios of 1.0, 2.0 and 2.5 were adopted so that different failure modes might be expected in the tests, where L is the specimen length; h is the depth of column cross-section.

Table 1 Mechanical properties of concrete

Usage of specimen	f_{cu} (MPa)	f_c (MPa)	E_c (MPa)	f_t (MPa)
L1, +4, T9	27.240	20.701	2.877×10^4	2.354
T1, +1, L4, T5	25.475	19.361	2.806×10^4	2.251
T3, T4, +2, +3	28.086	21.345	2.909×10^4	2.402
T8	22.813	17.330	2.685×10^4	2.091
L3, T7	24.880	18.908	2.781×10^4	2.216
L2, T2, T6	27.026	20.539	2.869×10^4	2.342

Table 2 Mechanical properties of steel and reinforcement materials (average values)

Steel form	Usage / type	Yield strength f_y (MPa)	Ultimate strength f_u (MPa)	Elasticity modulus E_s (MPa)
Steel shape	Web in the No. 5 steel channel	542.5	667.5	1.952×10^5
	Flange in the No. 5 steel channel	440.0	640.0	2.130×10^5
	25 mm-wide and 8 mm-thick steel plate	385.0	566.7	2.379×10^5
	50 mm-wide and 8 mm-thick steel plate	290.0	435.0	2.162×10^5
	50 mm-wide and 10 mm-thick steel plate	387.5	600.0	1.848×10^5
	50 mm-wide and 14 mm-thick steel plate	277.5	457.5	2.330×10^5
Steel plate	5 mm thickness	352.5	470.0	2.046×10^5
Reinforcing steel bar	6 mm in diameter	360.0	545.0	2.465×10^5
Iron wire	No. 8: 4.0 in diameter	246.7	338.3	1.450×10^5

Table 3 Experimental parameters and failure patterns of specimens

Code	Steel form	Loading angle	n^t	N^t (kN)	λ	f_{cu} (MPa)	ρ_{ss} (%)	ρ_s (%)	ρ_{sv} (%)	ρ_{sw} (%)	Failure mode
T1	T-shaped	flange	0.236	250.01	1.0	19.36	8.33	0.59	0.72	3.87	shear failure
T2	T-shaped	web	0.408	458.57	2.0	20.54	8.33	0.59	0.71	3.77	shear failure
T3	T-shaped	45°	0.584	682.27	2.5	21.35	8.33	0.59	0.72	3.74	flexural failure
T4	channel	flange	0.304	355.15	2.5	21.35	8.49	0	0.72	3.67	flexural failure
T5	channel	45°	0.398	421.63	1.0	19.36	8.49	0	0.72	3.99	shear failure
T6	channel	web	0.177	198.94	2.0	20.54	8.49	0	0.72	3.72	shear-bond failure
T7	solid-web	flange	0.441	456.33	2.0	18.91	11.21	0.59	0.72	0	flexural failure
T8	solid-web	45°	0.177	167.85	2.5	17.33	11.21	0.59	0.72	0	flexural failure
T9	solid-web	web	0.334	378.32	1.0	20.70	11.21	0.59	0.72	0	shear failure
L1	channel	engineering axis	0.193	218.61	1.0	20.70	5.39	0	0.72	3.99	shear failure
L2	channel	45°	0.447	502.41	2.0	20.54	5.39	0	0.72	3.72	flexural failure
L3	solid-web	engineering axis	0.526	544.28	2.0	18.91	7.55	0.59	0.72	0	flexural failure
L4	solid-web	45°	0.229	242.60	1.0	19.36	7.55	0.59	0.72	0	shear-flexural failure
+ 1	T-shaped	engineering axis	0.442	468.25	1.0	19.36	6.25	0.59	0.72	1.62	shear failure
+ 2	T-shaped	45°	0.651	760.55	2.5	21.35	6.25	0.59	0.72	3.07	flexural failure
+ 3	channel	engineering axis	0.462	539.74	2.5	21.35	7.18	0	0.72	3.75	flexural failure
+ 4	channel	45°	0.323	365.86	1.0	20.70	7.18	0	0.72	4.09	shear failure

In considerations of the available maximum loading capacity of the actuator and the conditions of the laboratory, the scale ratio of the specimens was finally determined as 1:3. All the column limb thicknesses were 240 mm with the sectional depth-thickness ratio of 3.5. Fig. 2 shows the cross-sectional sizes and the steel forms of SRC special shaped column specimens. The specimens

T4, T5, T6, L1, L2, +3 and +4 were configured with channel-shaped steel, which was banded with stirrups. The T-shaped steel was welded by steel flats which were fully double-sided along the vertical direction of steel skeletons. Q235 (the standard yield point is 235 MPa) steels and Hot rolled Plain Bar (HPB) (the standard yield point is 235 MPa) were used in this investigation. The mechanical properties of steel and reinforcement materials obtained from the material property tests are given in Table 2. The specimen design parameters are shown in Table 3, where ρ_{ss} is the shape steel content ratio in column cross-section, ρ_s is the longitudinal reinforcement steel bar content ratio in column cross-section, ρ_{sv} is the stirrup ratio by volume, ρ_{sw} is the diagonal steel flat ratio by volume.

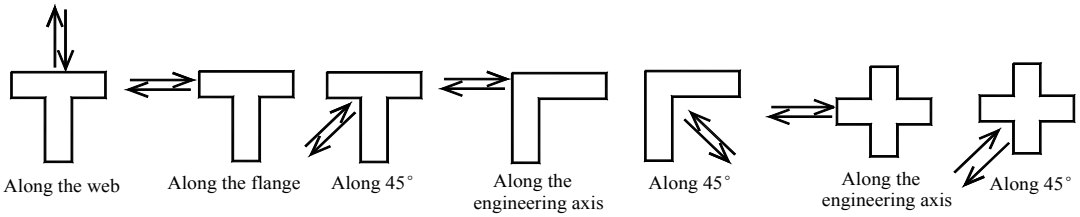

(a) Planar sketch of loading for special shaped columns

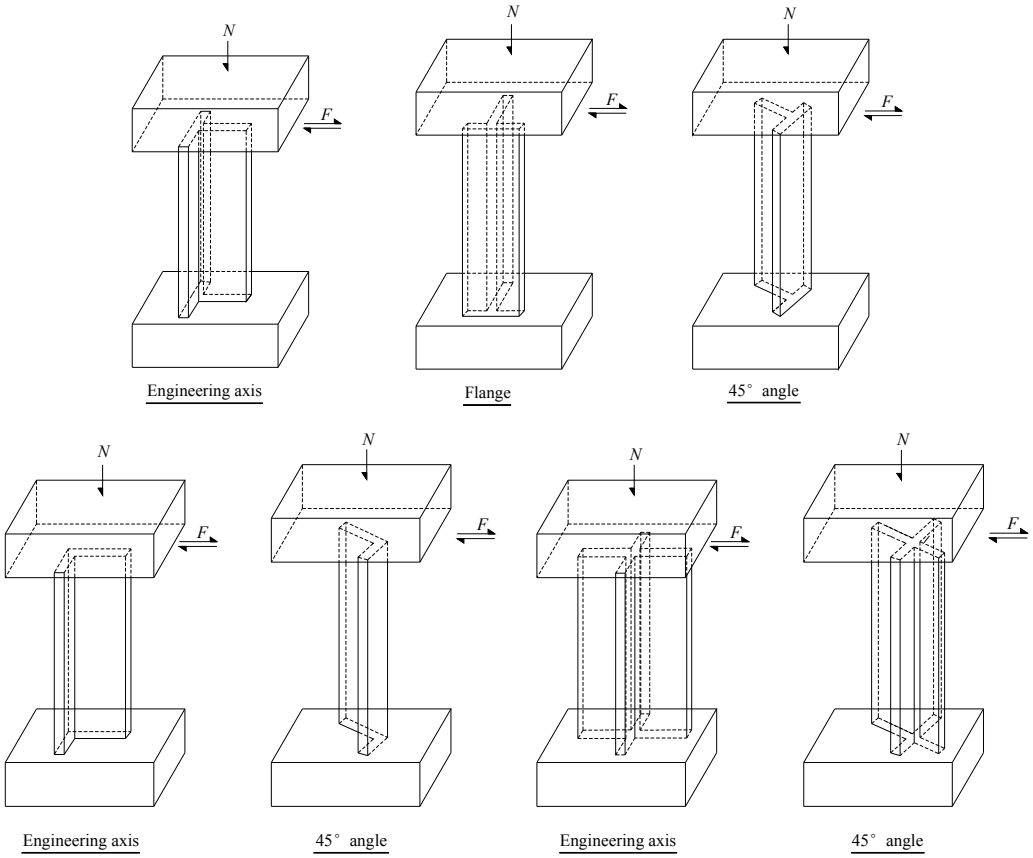

(b) Spatial loading diagram for specimens

Fig. 1 Loading angles for special shaped columns

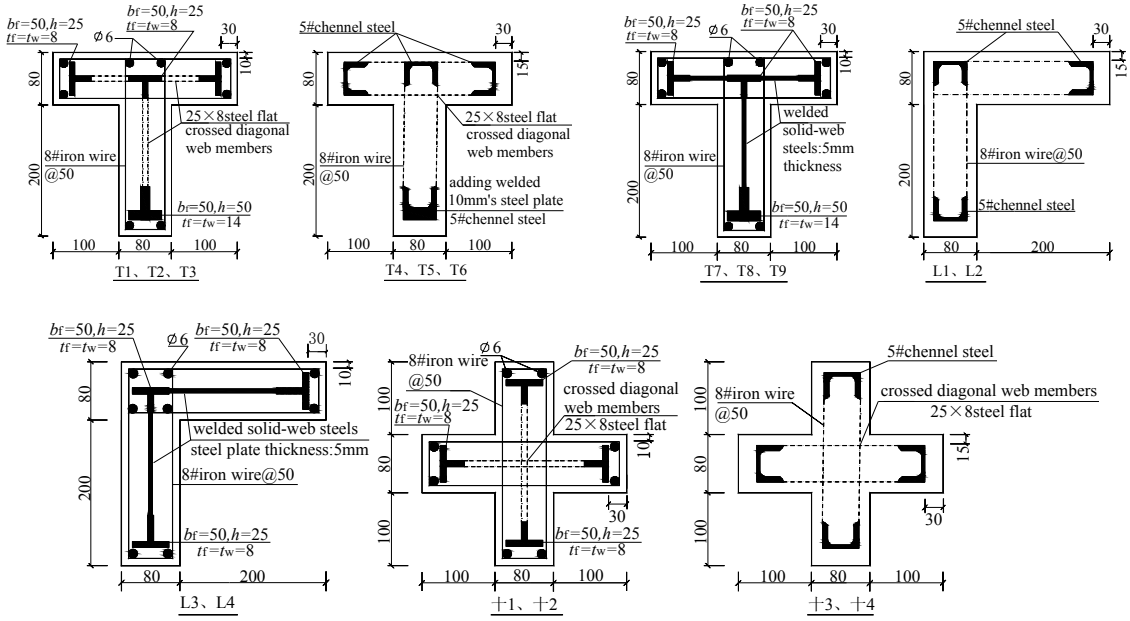

Fig. 2 Geometry and steel details of specimens

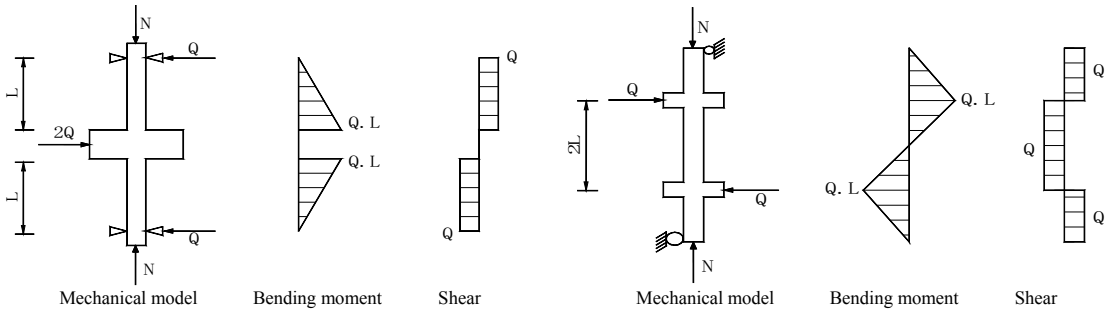

Fig. 3 Mechanical model for each loading device

Fig. 4 Test setup

2.2 Loading device

There are several test devices which can carry out the seismic behavior experiments for columns. For example, the simple-beam type, continuous beam type, cantilever column type and PCE type (PCE is the Japanese device for the pseudo-static experiment of structures) are the common loading devices for anti-seismic test (Kang and Gong 1997, Cao *et al*. 2005, Wei and Feng 1995, Legeron and Paultre 2000, Zhang and Wang 2000). In terms of force boundary conditions for actual structures, the PCE loading device can simulate the real force conditions more accurately than other loading devices. Early researchers who carried out the tests on the hysteretic behavior of RC special shaped columns had not adopted this loading device. Due to the asymmetry of special shaped column cross-sections, there was a phenomenon that both positive and negative directions of hysteretic loop were significantly asymmetric in the previous test results (Zhou *et al*. 2012, Cao *et al*. 2005). However, Chen *et al*. (2010) found that in spite of the asymmetric cross-sections of special shaped columns, the hysteretic performance of such columns was symmetric in the real structures through the mechanics analysis. As illustrated in Fig. 3, four mechanical models corresponding to the loading types present their bending moments and shear forces. Obviously, it can be seen that the PCE type matches the characteristics of column model between the layers well. Therefore, in order to simulate the actual force conditions of a structure, it is very necessary to employ the PCE loading device for anti-seismic tests of special shaped columns. Fig. 4 shows the PCE testing system in this investigation.

2.3 Loading procedure

During the test, the vertical load controlled by high-precision WY30B-V type hydraulic regulator was applied to the specimen and then maintained constant. Horizontal force was imposed using the force-control scheme repeated only once at each control point before the specimen yields, and then using the displacement-control scheme repeated three times at each control point after the specimen yields. Until the compression steels were yielded or the horizontal load decreased to the 70% of the maximum, the test was finished. For all the specimens, the deformation of the upper column end was measured by LVDT.

3. Test results and analysis

3.1 Failure characteristics

All the specimens behaved in a relatively ductile manner and the testing proceeded in a smooth and controlled fashion. Fig. 5 illustrates the destruction regional distribution and failure

characteristics of SRC special shaped columns. Due to the irregular sections of SRC special shaped columns, there are several characteristics described as follows. For the T-shaped columns loaded along the web, the failure modes were either the shear failure or the flexural failure, and the destruction zone was mainly in the web, however, the flange was almost not damaged or it was much less damage compared with the web zone. When the specimens were loaded along the axis of the flange, the destruction zone of T-shaped columns were mainly in the flange. For the flexural failure, the concrete at the upper and lower ends of specimens were crushed. While for the shear failure, the destruction area mainly concentrated near the interface between flange and web. Regardless of failure modes, the destruction of web in the specimens was not obvious, and even did not happen to damage. The main reason is that when the shear failure appears, the web shearing cross-section area is significantly increased, so that its shear stress becomes small. For the flexural failure, the normal stress in the T-shaped cross-section was very small due the web was located near the neutral axis. When the specimens were loaded along the 45° angle, whether the shear failure or the flexural failure, the serious destruction parts occurred within the single resistance flange. For the shear failure, the flank flange was single sheared, while the other flank flange was sheared together with the web (which led to enlarge the area), so that the shear stress was rather small. While for the flexural failure, the areas of concrete and steel where pressure applied on was much smaller than the other side, so that it was badly damaged.

For the L-shaped columns, when they were loaded along the engineering axis, the failure modes of specimens were similar to those of T-shaped columns which were loaded along the web. However, it can be seen that the flange which is perpendicular to the loading direction is almost no damage in the specimens. When appearing the flexural failure along the 45° angle loading, there was a serious destruction zone occurring at the junction of web and flange. The main reason is that the areas of compression shape steel and concrete at this region are relatively small, so that the shear capacity of the specimens can be weakened.

For the cross-shaped columns, when the specimens were loaded along the engineering axis, their failure models were similar to the T-shaped columns loaded along the flange. What's more, the web that was vertical to the loading direction was almost not damaged. When appearing the shear failure along the 45° angle loading, the specimens firstly cracked at the junction of two engineering axis, and the failure at this region was the most serious. The reason is that the shear area of this region is very small and it is near the neutral axis, hence, it must be the weak location for bearing the shear stress.

3.1 Failure characteristics

All the specimens behaved in a relatively ductile manner and the testing proceeded in a smooth and controlled fashion. Fig. 5 illustrates the destruction regional distribution and failure characteristics of SRC special shaped columns. Due to the irregular sections of SRC special shaped columns, there are several characteristics described as follows. For the T-shaped columns loaded along the web, the failure modes were either the shear failure or the flexural failure, and the destruction zone was mainly in the web, however, the flange was almost not damaged or it was much less damage compared with the web zone. When the specimens were loaded along the axis of the flange, the destruction zone of T-shaped columns were mainly in the flange. For the flexural failure, the concrete at the upper and lower ends of specimens were crushed. While for the shear failure, the destruction area mainly concentrated near the interface between flange and web. Regardless of failure modes, the destruction of web in the specimens was not obvious, and even

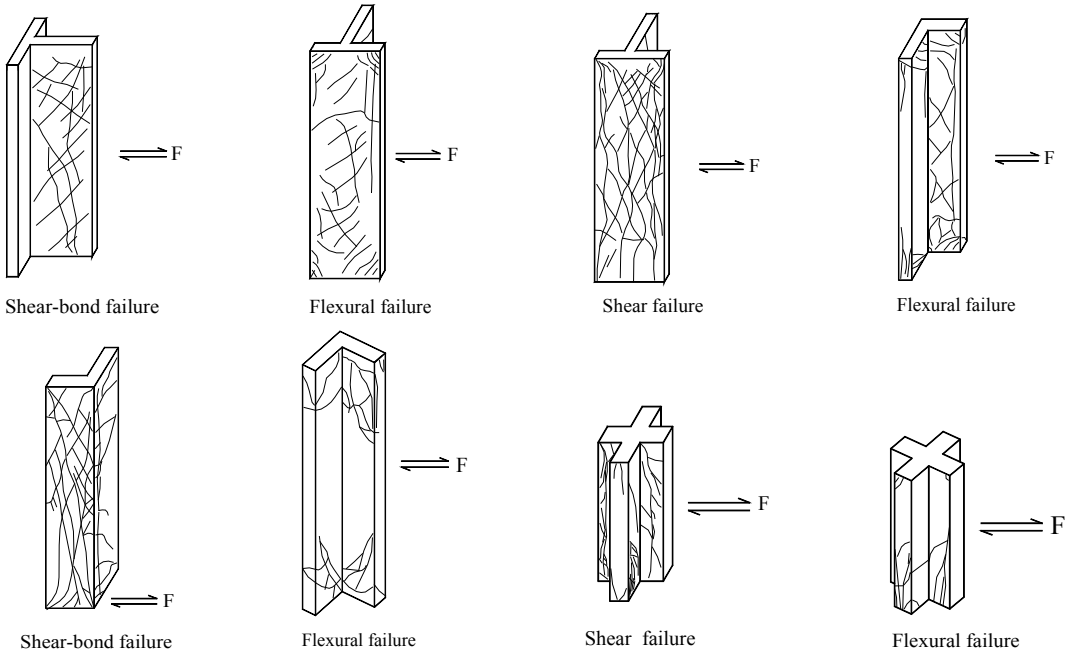

Fig. 5 Main destruction regional distribution and characteristics for SRCSS columns

did not happen to damage. The main reason is that when the shear failure appears, the web shearing cross-section area is significantly increased, so that its shear stress becomes small. For the flexural failure, the normal stress in the T-shaped cross-section was very small due the web was located near the neutral axis. When the specimens were loaded along the 45° angle, whether the shear failure or the flexural failure, the serious destruction parts occurred within the single resistance flange. For the shear failure, the flank flange was single sheared, while the other flank flange was sheared together with the web (which led to enlarge the area), so that the shear stress was rather small. While for the flexural failure, the areas of concrete and steel where pressure applied on was much smaller than the other side, so that it was badly damaged.

For the L-shaped columns, when they were loaded along the engineering axis, the failure modes of specimens were similar to those of T-shaped columns which were loaded along the web. However, it can be seen that the flange which is perpendicular to the loading direction is almost no damage in the specimens. When appearing the flexural failure along the 45° angle loading, there was a serious destruction zone occurring at the junction of web and flange. The main reason is that the areas of compression shape steel and concrete at this region are relatively small, so that the shear capacity of the specimens can be weakened.

For the cross-shaped columns, when the specimens were loaded along the engineering axis, their failure models were similar to the T-shaped columns loaded along the flange. What's more, the web that was vertical to the loading direction was almost not damaged. When appearing the shear failure along the 45° angle loading, the specimens firstly cracked at the junction of two engineering axis, and the failure at this region was the most serious. The reason is that the shear area of this region is very small and it is near the neutral axis, hence, it must be the weak location for bearing the shear stress.

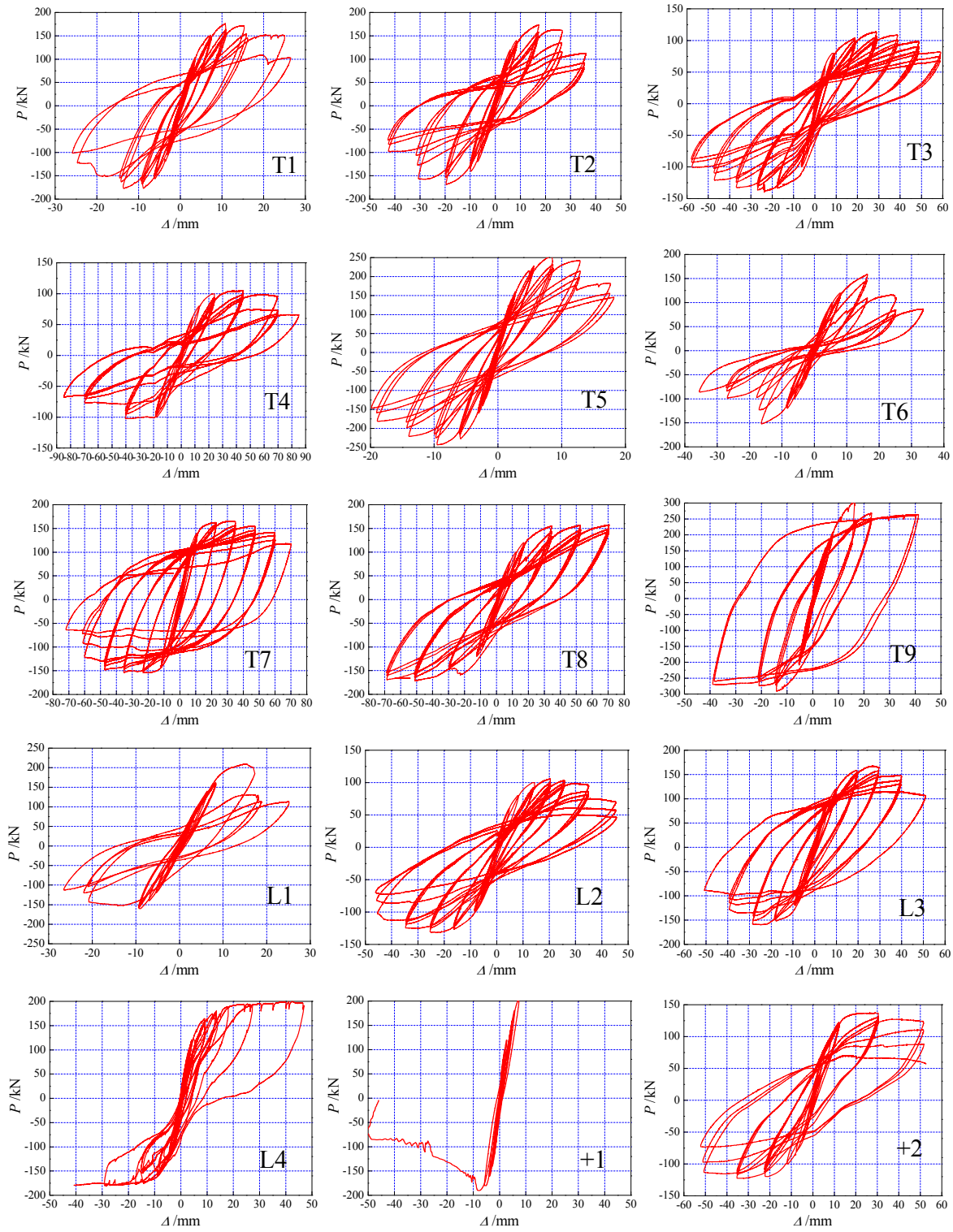

Fig. 6 Hysteretic curves of specimens

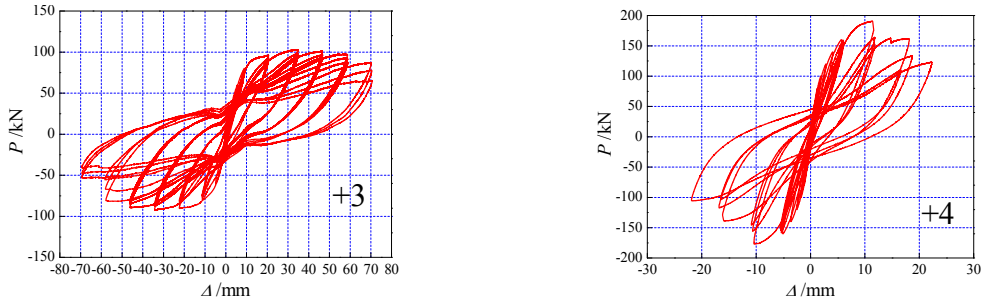

Fig. 6 Continued

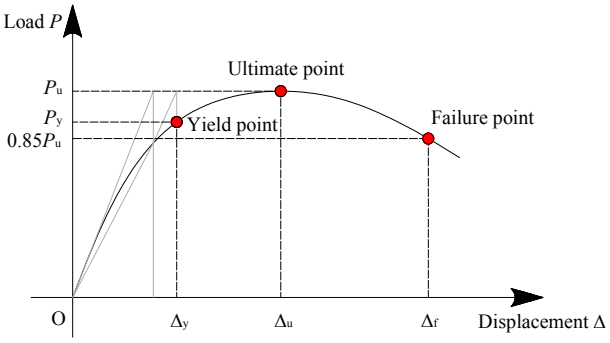

Fig. 7 Characteristic points on load–displacement curve

3.3 Ductility

Ductility is one of the most significant indexes to evaluate the seismic performance of a structure or structural member. The displacement ductility coefficient μ can be calculated as the ratio of failure displacement Δ_f (Δ_f is defined as the maximum displacement corresponding to the load no less than $0.85P_u$) to the yield displacement Δ_y, which is determined by the general yield bending moment method. As Nie *et al*. (2008) suggested, the yield point (P_y, Δ_y) can be determined using the graphical method as shown in Fig. 7. The average displacement ductility coefficients of all the specimens listed in Table 4 (the average value of positive $+\mu$ and negative $-\mu$) indicate that there is a good ductility for this new type of columns. In addition, it can be clearly seen that the displacement ductility coefficients of test specimens are almost the same with SRC rectangle columns (Zhou and Liu 2010, Ma *et al*. 2013), and the μ of test specimens is over 3.0, indicating that the deformation ability of SRC special shaped columns is good enough under earthquake action.

4. Axial compression ratio limit values

Up to now, there have been mainly two kinds of theoretical methods to determine the limit values of axial compression ratio for SRC structural columns. One theory is on the basis of balanced failure and the other theory is on the basis of superposition.

4.1 Calculation based on balanced failure

4.1.1 Calculation analysis

Actually, the limit values of axial compression ratio calculated by balanced failure (transition from small eccentric compression to large eccentric compression) is to restrict the axial compression coefficient of structural column components under the condition of appearing the large eccentric compressive failure but with a good ductility, so that sufficient deformation ability of a structure can be ensured under seismic action. As suggested by Chen *et al*. (2013), there are two kinds of failure patterns of normal section for SRC special shaped columns according to the experimental studies, such as the failure under large eccentric compression and the failure under small eccentric compression. In addition, the whole cross-section of shape steel in SRC structures cannot be completely yielded due the existence of shape steel web, even if the specimens are close to failure.

Currently, there is no uniform definition for balanced failure state of SRC columns that is universally accepted. One view is that the tensile reinforcement is yielded, and meanwhile, the concrete strain at the edge of compressive zone reaches the ultimate compressive value at the same time, while the other view is that the flange of tensile shape steel is yielded, and meanwhile, the concrete strain at the edge of compressive zone reaches the ultimate compressive value at the same time. In this investigation, the balanced failure of SRC special shaped columns is defined that the outside-edge fiber of tensile shape steel is yielded, and meanwhile, the concrete strain at the edge of compressive zone reaches the ultimate compressive value due to the irregular cross-section and the shape steel configuration of these components. Based on the before-mentioned judgment criteria, an equilibrium equation of internal force can be derived as follows

$$N_b = \sum \sigma_{ci} A_{ci} + \left(\sum \sigma_{sj} A_{sj} + \sum \sigma_{ssj} A_{ssj} \right) \tag{3}$$

where $\Sigma\sigma_{ci}A_{ci}$ is the resultant force of concrete in the compressive zone of cross-section; $\Sigma\sigma_{sj}A_{sj}$ + $\Sigma\sigma_{ssj}A_{ssj}$ is the resultant force of both tensile and compressive reinforcement and shape steel.

Hence, a formula of axial compression ratio is naturally formed by substituting Eq. (3) into Eq. (2).

$$n_b^c = \frac{\sum \sigma_{ci} A_{ci} + \left(\sum \sigma_{sj} A_{sj} + \sum \sigma_{ssj} A_{ssj} \right)}{f_c A_c + f_s A_{ss}} \tag{4}$$

It can be seen from Eq. (4) that it is rather tedious to calculate the axial compression ratio of SRC special shaped columns due to the existence of a crowd of influence parameters; especially, it is hard to carry out the computational process via hand computation due to the irregular cross-section of special shape columns. Hence, the numerical integration method in this paper is used to calculate the axial compression ratio limit values through finite element program. The process of numerical integration is stated below.

(1) Assumptions

- The plane sections remain plane after bending, resulting in a linear distribution of strains; namely, it is the flat section assumption;
- The tensile stress of concrete is neglected;
- The Rüsch (1960) stress-strain relationship is used for describing the constitutive relationship of concrete;

- The ideal elastoplastic model stress-strain relationship is used for the reinforcement and shape steel.

(2) Establishment of coordinate system

As shown in Fig. 8, two sets of coordinate system are used to obtain the cross-sectional information of SRC cross-shape columns. Obviously, the global coordinate system named *XOY* is built for the cross-section of special shape columns, while the local coordinate system named *xoy* is established for the shape steels. In addition, in order to guarantee the universality of program, the entire column section is located in the first quadrant of *XOY* system. Hence, different types of cross-sections for special shape columns can be determined by controlling the length of B_i (i = 0, 1, 2, 3, 4, 5): (1) if $B_5 = B_1/2$, the cross-section is a T-shaped type; (2) if $B_2 = B_0/2$ and $B_5 = B_1/2$ or $B_4 = B_1/2$ and $B_2 = B_0/2$, the cross-section is a L-shaped type.

(3) Element division

- Each reinforcement is seen as a unit;
- Concrete and shape steels are divided into small squares, respectively; especially, the size of grid element of shape steel is not exceeding 1 mm;

(4) Element strain and stress

According to the flat section assumption, the sectional curvature in the case of occurring the balanced failure can be calculated as

$$\varphi = \frac{\varepsilon_{cu} + f_s / E_s}{R_2 - R_1} \tag{5}$$

where R_1 is the recent distance from the origin of coordinates to the point of compressive concrete; R_2 is the furthest distance from the origin of coordinates to the point of tensile shape steel. The schematic plots of R_1 and R_2 are shown in Fig. 9. It can be clearly seen that the values of R_1 and R_2 are determined by the sectional coordinate values of concrete element and shape steel element. ε_{cu} = 0.0033 is the ultimate compressive strain of concrete; E_s is the elasticity modulus of shape steel.

For any loading angle, plotting a line through each element centroid is employed as a normal vector parallel to the loading direction. As a result, the distance between this line and the origin of coordinates can be calculated as

$$R = x\cos\theta + y\sin\theta \tag{6}$$

Then the strain equations of concrete element, reinforcement element and shape steel element can be obtained as follows, respectively:

For the concrete element

$$\varepsilon_{ci} = 0.0033 - \varphi(x_i\cos\theta + y_i\sin\theta) - R_1 \tag{7}$$

For the reinforcement element

$$\varepsilon_{si} = 0.0033 - \varphi(x_i\cos\theta + y_i\sin\theta) - R_1 \tag{8}$$

For the shape steel element

$$\varepsilon_{ssi} = 0.0033 - \varphi(x_i\cos\theta + y_i\sin\theta) - R_1 \tag{9}$$

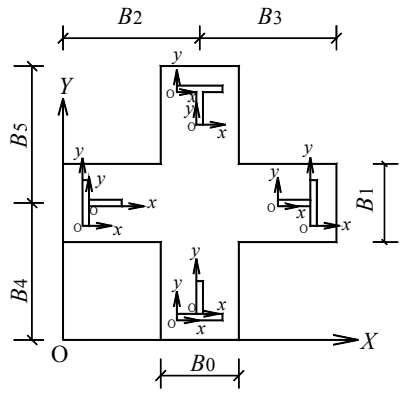

Fig. 8 Coordinate system arrangement

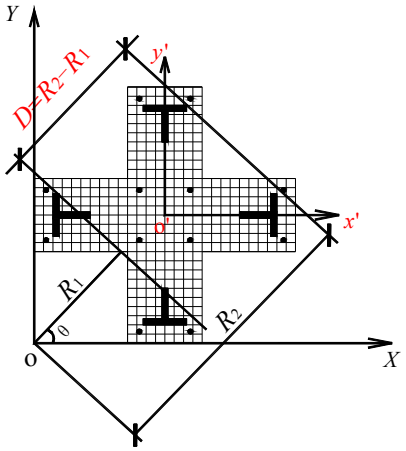

Fig. 9 Element divisions of cross-section

As for the stresses of concrete element, reinforcement element and shape steel element, they can be obtained according to their constitutive relationships.

4.1.2 Effect of loading angle

Seismic-induced direction has important influence on the failure mechanism of a structure column, especially, the limit value of axial compression ratio for a type of SRC special shaped column under different seismic-induced angles can be transformed due to the irregular cross-section. Table 4 lists the calculation results of axial compression ratio limit values for the test specimens subjected to different loading angels. It can be observed that there is a large difference for the same specimen under the action of loading angles. In addition, it is worth noting that the most unfavorable seismic-induced directions are not the same among cross-shaped, T-shaped and L-shaped columns: (1) for cross-shaped columns, the minimum value of limit of axial compression ratio is appearing in the situation of 45° loading angle; (2) for T-shaped and L-shaped columns, the minimum value of limit of axial compression ratio is appearing in the situation of 90° loading angle, indicating that the webs and flanges of T-shaped and L-shaped cross-sections are compressive and tensile, respectively.

4.1.3 Verification and discussion

It is necessary to examine the rationality of the theory based on balanced failure for calculating the limit values of axial compression ratio of SRC special shaped columns, and the judgment rules can be described that: (1) if test axial compression ratio is smaller than calculated limit value of axial compression ratio and $\mu \geq 3.0$, it can be concluded that the calculation results using the theory is credible; (2) if test axial compression ratio is larger than calculated limit value of axial compression ratio but $\mu \geq 3.0$, it can be concluded that the calculation results using the theory is incorrect.

The calculation results of n_b^c for all the specimens are shown in Table 5. It can be observed that the test axial compression ratios applying to the specimens T2 and T9 loaded along the web and the specimen L3 loaded along the engineering axis are significantly greater than their calculated limit values of axial compression ratio; however, the ductility of these specimens is still satisfying

the requirement of $\mu \geq 3$. The reason is that there is a defect that the contribution of shape steel in sharing the axial force cannot be reflected when the balanced failure theory is used to calculate the limit values of axial compression ratio for SRC special shaped columns. Here, a type of SRC rectangular columns configured with symmetric empty-web steel is taken as an example to

Table 4 Axial compression ratio limit values n_b^c for test specimens under different loading angles

Loading angle	T-shaped column			L-shaped column		Cross-shaped column	
	T-shaped steel	Channel-shaped steel	Solid-web steel	Channel-shaped steel	Solid-web steel	T-shaped steel	Channel-shaped steel
0°	0.712	0.785	0.713	1.246	1.101	0.636	0.824
22.5°	0.946	1.196	0.939	1.023	0.902	0.547	0.744
45°	0.739	0.991	0.691	0.811	0.616	0.534	0.742
67.5°	0.365	0.681	0.291	0.591	0.285	0.626	0.776
90°	0.069	0.399	-0.045	0.349	-0.116	0.636	0.824
112.5°	0.365	0.681	0.291	0.728	0.275	0.616	0.776
135°	0.739	0.991	0.691	1.202	0.759	0.534	0.742
157.5°	0.946	1.196	0.939	0.802	0.408	0.547	0.744
180°	0.712	0.785	0.713	0.463	0.241	0.636	0.824
202.5°	0.539	0.858	0.075	0.734	0.631	0.547	0.744
225°	0.401	0.977	0.454	0.971	0.926	0.534	0.742
247.5°	0.675	1.091	0.746	1.171	1.125	0.626	0.776
270°	0.747	1.146	0.836	1.368	1.249	0.636	0.824
292.5°	0.675	1.091	0.746	0.993	1.039	0.616	0.776
315°	0.401	0.977	0.454	0.458	0.519	0.534	0.742
337.5°	0.539	0.858	0.075	0.935	0.991	0.547	0.744
360°	0.712	0.785	0.713	1.246	1.101	0.636	0.824

Table 5 Ductility coefficients and axial compression ratio limit values for test specimens (calculated by balanced failure theory)

Code	T1	T2	T3	T4	T5	T6	T7	T8	T9
μ	3.71	3.44	4.77	3.01	3.27	2.28	5.78	7.04	4.55
n^t	0.236	0.408	0.584	0.304	0.398	0.177	0.441	0.177	0.334
n_b^c	0.702	**0.069**	0.739	0.785	0.991	0.399	0.713	0.691	**-0.045**
n_t / n_b^c	0.336	5.913	0.790	0.387	0.402	0.444	0.619	0.256	-7.422
Code	L1	L2	L3	L4	+ 1	+ 2	+ 3	+ 4	
μ	2.03	3.71	3.47	6.29	1.76	4.78	6.98	3.89	
n^t	0.193	0.447	0.526	0.229	0.442	0.651	0.462	0.323	
n_b^c	0.349	0.811	**-0.116**	0.616	0.636	0.634	0.824	0.742	
n_t / n_b^c	0.553	0.551	-4.534	0.372	0.695	1.027	0.561	0.435	

illustrate the above idea. When the balanced failure occurs, both tensile and compressive shape steels are yielded, so that the internal forces can be cancelled out. Based on this situation, the axial compression ratio limit values of SRC rectangular columns using balanced failure theory is equal to that of RC rectangular columns with the same cross-sectional area, but the fact is that the ductility and seismic performance of SRC rectangular columns configured with symmetric empty-web steel are superior to those of the same cross-sectional RC columns, indicating that the axial compression ratio limit values of SRC rectangular columns is larger than that of RC columns. In addition, it is illogical that the negative and diminutive limit values of axial compression ratio (such as -0.045, -0.116 and 0.069) are appearing in the calculation results. In view of this, it can be concluded that the balanced failure theory is not the best calculation method for SRC special shaped columns.

4.2 Calculation based on superposition theory

4.2.1 Background and procedure

Actually, the calculation idea of Eq. (2) is based on the superposition theory, which means that the vertical axis force contributed by the concrete and the shape steel are calculated separately, and then the two forced components are superposed to obtain the column vertical axis force. Based on this method, the axial load limit of SRC columns can be expressed as

$$N = n_c f_c A_c + n_s f_s A_{ss} \tag{10}$$

where n_c is the axial force distribution coefficient of concrete, n_s is the axial force distribution coefficient of shape steel. In AIJ standard (2001), $n_c = 1/3$ and $n_s = 2/3$.

In order to gain the values of n_c and n_s, Qiang (2002) put forward the vertical axis force calculation model of SRC rectangular columns configured with solid-web steel.

$$N = 0.747 f_c A_c + 0.771 f_s A_{ss} \tag{11}$$

In addition, Ye *et al*. (1997) carried out a series of experimental and theoretical studies on nine SRC rectangular columns configured with empty-web steel, and proposed the vertical axis force calculation model below.

$$N = 0.64 f_c A_c + 0.751 f_s A_{ss} \tag{12}$$

where the factors of $0.747, 0.771$ in Eq. (11) and $0.64, 0.75$ in Eq. (12) are obtained by mathematical regression in each test results.

It is worth noting in Eqs. (11) and (12) that the shape steel configuration in SRC rectangular columns is symmetric in column cross-section, so that SRC special shaped columns do not belong to this category due to their irregular cross-sections and unsymmetrical shape steel configuration. However, according to the experimental observation, the test results show that the failures of SRC special shaped columns are mainly appearing at the column limbs (which are parallel to the loading direction). Hence, the seismic behavior of special shaped columns can be seen as the characteristic of rectangular columns subjected to the loading direction of paralleling to the special shaped column limb, so that the cross-sections of special shaped columns can be simplified as a rectangular cross section. For the issue of unsymmetrical shape steel configuration, the symmetrization method can be used to restructure the sectional shape steel as suggested by Xue *et*

al. (2012). In this paper, the shape steel recombination is based on the principle of minimum shape steel ratio between tension and compression zones. As an example, Fig. 10 illustrates the simplification process of T-shaped cross-section and the reconstruction of shape steel configuration.

For SRC T-shaped and L-shaped columns configured with solid-web steel, the limit values of axial compression ratio can be calculated as

$$n_s^c = \frac{0.747 f_c A_c^s + 0.771 f_s A_{ss}^s}{f_c A_c + f_s A_{ss}} \tag{13}$$

While for SRC T-shaped and L-shaped columns configured with empty-web steel, the limit values of axial compression ratio can be expressed as

$$n_s^c = \frac{0.64 f_c A_c^s + 0.751 f_s A_{ss}^s}{f_c A_c + f_s A_{ss}} \tag{14}$$

where A_s^c is the concrete area of column limb which is parallel to the loading direction; A_{ss}^s is the corrected shape steel area of column limb which is parallel to the loading direction.

Due to the symmetry of cross-shaped columns, the shape steel configuration in the cross-section is also symmetrical, so that there is no need to simplify the cross-section and the shape steel configuration. For SRC cross-shaped columns configured with solid-web steel, the limit values of axial compression ratio can be calculated as

$$n_s^c = \frac{0.747 f_c A_c + 0.771 f_s A_{ss}}{f_c A_c + f_s A_{ss}} \tag{15}$$

While for SRC cross-shaped columns configured with empty-web steel, the limit values of axial compression ratio can be expressed as

$$n_s^c = \frac{0.64 f_c A_c + 0.751 f_s A_{ss}}{f_c A_c + f_s A_{ss}} \tag{16}$$

4.2.2 Verification and discussion

Table 6 lists the calculated limit values of axial compression ratio n_s^c and the test axial compression ratio n^t for the specimens with $\mu > 3.0$ (this ductility requirement is to ensure the structural deformation, so that the specimens T6, L1 and + 1 are not discussed here due to their μ(s) are no more than 3.0). It can be seen that the test axial compression ratio subjecting to the specimens is basically close to or smaller than the calculated axial compression ratio limit values, and the average value of n^t/n^c is 0.737. In addition, in terms of rationality, there are no negative and diminutive values when using the superposition method, indicating that the superposition theory is more suitable for SRC special shaped columns.

In this paper, the design limit values of axial compression ratio for SRC special shaped columns under the second seismic grade is determined based on the superposition theory. Then, the design limits for SRC special shaped columns under the first and third seismic grades can be finalized by drawing from the literature GB50010-2010 (2010), which means that the limit values

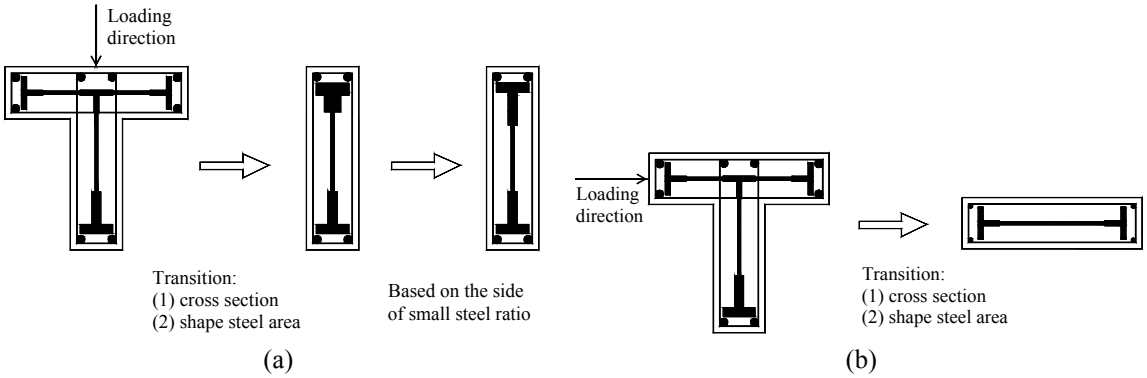

Fig. 10 Simplification of T-shaped SRC column section

Table 6 Axial compression ratio limit values for test specimens (calculated by superposition theory)

Code	T1	T2	T3	T4	T5	T7	T8	T9	L2	L3	L4	+ 2	+ 3	+ 4
n^t	0.236	0.408	0.584	0.304	0.398	0.441	0.177	0.334	0.447	0.526	0.229	0.651	0.462	0.323
n_b^c	0.586	0.499	0.497	0.472	0.475	0.655	0.513	0.509	0.441	0.445	0.445	0.693	0.705	0.706
n_t/n_b^c	0.403	0.817	1.175	0.644	0.838	0.673	0.345	0.656	1.014	1.182	0.515	0.939	0.655	0.458

Table 7 Design limit values of axial compression ratio for SRC special shaped columns under different seismic levels

Seismic level	First grade	Second grade	Third grade
L-shaped SRC column	0.4	0.5	0.6
T-shaped SRC column	0.4	0.5	0.6
Cross-shaped SRC column	0.6	0.7	0.8

Table 8 Design limit values of axial compression ratio for RC special shaped columns under different seismic levels

Seismic level	Second grade	Third grade	Forth grade
L-shaped SRC column	0.5	0.6	0.7
T-shaped SRC column	0.55	0.65	0.75
Cross-shaped SRC column	0.6	0.7	0.8

of axial compression ratio under the first level can be determined by subtracting the value of 0.1 from the second level, and the limit values of axial compression ratio under the third level can be determined by adding the value of 0.1 from the second level. Table 7 shows the design limit values of axial compression ratios for SRC special shaped columns under the first, second and third seismic grades.

4.3 Example analysis

As shown in Table 8, the design limit values of axial compression ratio for RC special shaped columns under different seismic levels is specified in Chinese specification JGJ 149-2006 (2006). Even though the limit values can be equal between RC and SRC special shaped columns, there will be a wide difference for the ultimate axial load bearing capacities of them, due to their different calculation methods ($n = N/f_cA$, for RC special shaped columns). Here, the following example can illustrate the effect of shape steel for its strength contribution.

Example: Special shaped column structure is employed to build a high-rise building, and the seismic level is the second grade. The geometry and concrete information about L-shaped cross-section is described as follows: (1) the limb thickness is 240 mm; (2) ratio of limb height to limb thickness is 3.5; (3) the concrete design strength grade is C40. Two sets of scheme are used to design and check the ultimate axial bearing capacity of L-shaped column without exceeding the limit value of axial compression ratio.

- Scheme one is the RC special shaped columns:

$$N^{RC} = nf_c A = 0.5 \times 19.1 \times 345600 = 3300.5 \text{ kN};$$

- Scheme two is the SRC special shaped columns with $\rho_{ss} = 7\%$ and Q235 shape steel used:

$$N^{SRC} = n(f_c A_c + f_{ss} A_{ss}) = 0.5 \times [19.1 \times 345600 \times (1 - 0.07) + 235 \times 345600 \times 0.07] = 5912 \text{ kN};$$

- Comparison ratio: $\dfrac{N^{SRC} - N^{RC}}{N^{RC}} = \dfrac{5912 - 3300.5}{3300.5} \times 100\% = 79.1\%.$

Even if both SRC and RC special shaped columns have the same axial compression ratio, the comparison result shows that under the same condition of cross-sectional area, the axial load bearing capacity of SRC special shaped columns is much larger than that of RC special shaped columns due to the configuration of shape steel, indicating that the application range of SRC special shaped columns is much wider than that of RC special shaped columns.

5. Conclusions

An experimental study has been presented to investigate the hysteretic behavior of SRC (steel reinforced concrete) special shaped columns, and a total of 17 specimens have been prepared and tested in this study. Based on the test results, numerical calculation and theoretical analysis have been employed to investigate the limit values of axial compression ratio for SRC special shaped columns. The following important conclusions are obtained.

(1) The major failure modes of SRC special shaped columns are the shear failure, flexural failure, shear-bond failure and shear-flexural failure. Specimens with small shear-span ratio are mainly prone to appear the failure mode of shear deformation.
(2) Compared with the previous test results, the biggest difference in this test is that the hysteretic curves of all the specimens conducted on PCE loading device are symmetrical in positive and negative loading directions, which confirms the correctness of the theoretical analysis.

(3) The hysteretic curves of the specimens configured with solid-web steel are much plumper than those of the specimens configured with empty-web steel. The displacement ductility coefficients of test specimens are almost over 3.0 at failure, indicating that the deformability of SRC special shaped columns is better to apply them in the seismic region.
(4) The numerical integration method showed that 45° loading angle is against the cross-shaped columns and 90° loading angle is against the T-shaped and L-shaped columns, respectively.
(5) Compared with the balanced failure theory, the superposition theory on calculating the limit values of axial compression ratio is more suitable for SRC special shaped columns.
(6) The design limit values of axial compression ratio under different seismic grades are proposed for SRC special shaped columns: for L-shaped column and T-shaped column, 0.4, 0.5 and 0.6 are corresponding to the first grade, second grade and third grade, respectively; for cross-shaped column, 0.6, 0.7 and 0.8 are corresponding to the first grade, second grade and third grade, respectively.
(7) By considering the effect of shape steels, an example analysis showed that the ultimate axial load of SRC L-shaped column is 79.1% larger than that of RC L-shaped column due to the contribution of shape steel.

Acknowledgments

The authors would like to thank the Natural Science Foundation of China (No: 50908057 and 51268004), the Open Project of Guangxi Key Laboratory of Disaster Prevention and Structural Safety (No: 2012ZDX10) and Innovation Project of Guangxi Graduate Education (No: YCBZ2012005). The founding and support from the above projects are greatly acknowledged.

References

AIJ (Architectural Institute of Japan) (2001), Standards for structural calculation of steel reinforced concrete structures. [In Japanese]
Cao, W.L., Huang, X.M. and Song, W.Y. (2005), "Experiment and non-linear element analyses of seismic behavior of short specially shaped columns with crossed reinforcing bars", *J. Build. Struct.*, **26**(3), 30-37. [In Chinese]
Chen, Z.P., Xue, J.Y., Zhao, H.T. and Shao, Y.J. (2010), "Research on mechanics behavior of steel reinforced concrete special-shaped columns", *J. Xi'an Univ. Architect. Technol.* (*Natural Science Edition*), **42**(3), 329-334. [In Chinese]
Dundar, C. and Sahin, B. (1993), "Arbitrarily shaped reinforced concrete members subjected to biaxial bending and axial load", *Comput. Struct.*, **49**(4), 643-662.
GB 50010-2010 (2010), Code for design of concrete structures, China Architecture and Building Press, Beijing, China. [In Chinese]
GB 50011-2010 (2010), Code for seismic design of buildings, China Architecture and Building Press, Beijing, China. [In Chinese]
Hsu, T.C. (1989), "T-shaped reinforced concrete members under biaxial bending and axial compression", *ACI Struct. J.*, **86**(4), 460-468.
JGJ 149-2006 (2006), Technical specification for concrete structures with specially shaped columns, China Architecture and Building Press, Beijing, China. [In Chinese]
JGJ 138-2001 (2001), Technical specification for steel reinforced concrete composite structures, China

Architecture and Building Press, Beijing, China. [In Chinese]
Kang, G.Y. and Gong, C.J. (1997), "Shear properties of T and L-shaped section frame columns under monotonic and horizontal low cyclic loadings", *J. Build. Struct.*, **18**(5), 22-31. [In Chinese]
Legeron, F. and Paultre, P. (2000), "Behavior of high-strength concrete columns under cyclic flexure and constant axial load", *ACI Struct. J.*, **97**(4), 591-601.
Li, J., Wu, J.Y., Zhou, D.Y. and Nie, L.P. (2002), "Experimental research on wide flange specially shaped section columns subjected to cyclic loading", *J. Build. Struct.*, **23**(1), 9-14. [In Chinese]
Ma, H., Xue, J.Y., Zhang, X.C. and Luo, D.M. (2013), "Seismic performance of steel-reinforced recycled concrete columns under low cyclic loads", *Construct. Build. Mater.*, **48**(11), 229-237.
Mallikarjuna and Mahadevappa, P. (1992), "Computer aided analysis of reinforced concrete columns subjected to axial compression and bending-I L-shaped sections", *Comput. Struct.*, **44**(5), 1121-1138.
Marin, J. (1979), "Design aids for L-shaped reinforced concrete columns", *ACI J. Proceedings*, **76**(11), 1197-1216.
Nie, J.G., Qin, K. and Cai, C.S. (2008), "Seismic behavior of connections composed of CFSSTCs and steel-concrete composite beams: finite element analysis", *J. Construct. Steel Res.*, **64**(6), 680-688.
Patton, M.L. and Singh, K.D. (2012), "Numerical modeling of lean duplex stainless steel hollow columns of square, L-, T-, and +-shaped cross sections under pure axial compression", *Thin-Wall. Struct.*, **53**(4), 1-8.
Qiang, J.Y. (2002), *Experimental Study on Seismic Behavior and Distribution Axial Force of Truss Type Steel Reinforced Concrete Columns*, Southwest Jiaotong University, Chengdu, China. [In Chinese]
Ramamurthy, L. and Khan, T.A. (1983), "L-shaped column design for biaxial eccentricity", *J. Struct. Eng. ASCE*, **109**(8), 1903-1917.
Rüsch, H. (1960), "Researches toward a general flexural theory for structural concrete", *ACI J. Proceedings*, **57**(7), 1-28.
Sinha, S.N. (1996), "Design of cross (+) section of column", *Ind. Concrete J.*, **70**(3), 153-158.
Tokgoz, S. and Dundar, C. (2012), "Tests of eccentrically loaded L-shaped section steel fibre high strength reinforced concrete and composite columns", *Eng. Struct.*, **38**(5), 134-141.
Tsao, W.H. and Hsu, C.T.T. (1993), "A nonlinear computer analysis of biaxially loaded L-shaped slender reinforced concrete columns", *Comput. Struct.*, **49**(4), 579-588.
Wang, Q.T. and Chang, X. (2013), "Analysis of concrete-filled steel tubular columns with "T" shaped cross section (CFTTS)", *Steel Compos. Struct., Int. J.*, **15**(1), 41-55.
Wei, Y. and Feng, J.P. (1995), "Investigation on L-shaped reinforced concrete members with flexure and axial force under cyclic loading", *J. South China Univ. Technol.* (*Natural Science*), **23**(3), 44-50.
Wsu, C. (1985), "Biaxially loaded L-shaped reinforced concrete columns", *J. Struct. Eng. ASCE*, **111**(12), 2576-2595.
Wu, B. and Xu, Y.Y. (2009), "Behavior of axially-and-rotationally restrained concrete columns with '+'-shaped cross section and subjected to fire", *Fire Safe. J.*, **44**(2), 212-218.
Xu, Y.Y. and Wu, B. (2009), "Fire resistance of reinforced concrete columns with L-, T-, and +-shaped cross-sections", *Fire Safe. J.*, **44**(2), 869-880.
Xue, J.Y., Chen, Z.P., Zhao, H.T., Gao, L. and Liu, Z.Q. (2012), "Shear mechanism and bearing capacity calculation on steel reinforced concrete special-shaped columns", *Steel Compos. Struct., Int. J.*, **13**(5), 473-487.
Yau, C.Y., Chan, S.L. and So, A.K.W. (1993), "Biaxial bending design of arbitrarily shaped reinforced concrete columns", *ACI Struct. J.*, **90**(3), 269-278.
YB 9082-2006, (2007), *Technical Specification of Steel-reinforced Concrete Structures*, Metallurgical Industry Press, Beijing, China. [In Chinese]
Ye, L.P., Fang, E.H., Zhou, Z.H. and Liu, F.G. (1997), "Axial load limit for steel reinforced concrete columns", *J. Build. Struct.*, **18**(5), 43-50. [In Chinese]
Zhang, Y.F. and Wang, Z.H. (2000), "Seismic behavior of reinforced concrete shear walls subjected to high axial loading", *ACI Struct. J.*, **97**(5), 739-750.
Zhao, Y.J., Li, Z.X. and Chen, Y.X. (2004), "Research on limit values of axial compression ratios of specially shaped RC columns in case of 4th aseismic grade", *J. Build. Struct.*, **25**(3), 58-62. [In Chinese]

Zhou, X.H. and Liu, J.P. (2010), "Seismic behavior and strength of tubed steel reinforced concrete (SRC) short columns", *J. Construct. Steel Res.*, **66**(7), 885-896.
Zhou, T., Chen, Z.H. and Liu, H.B. (2012), "Seismic behavior of special shaped column composed of concrete filled steel tubes", *J. Construct. Steel Res.*, **75**(8), 131-141.
Zuo, Z.L., Cai, J., Yang, C. and Chen, Q.J. (2012a), "Eccentric load behavior of L-shaped CFT stub columns with binding bars", *J. Construct. Steel Res.*, **72**(5), 105-118.
Zuo, Z.L., Cai, J., Yang, C., Chen, Q.J. and Sun, G. (2012b), "Axial load behavior of L-shaped CFT stub columns with binding bars", *Eng. Struct.*, **37**(4), 88-98.

BU